Proceedings of the 11th ICPMG 2026
11th International Conference on Physical Modelling in Geotechnics
8-12 June 2026, Zurich, Switzerland

Centrifuge modeling of artesian response in silty-interlayered deep sandy deposits: Influence of underlying sand thickness

Y. Wu, Y. Zhao*, Y. Xiang, Q. Ma, Y. Zhou
Zhejiang University, Hangzhou, China, wuyigeotech@zju.edu.cn, zhao_yu@zju.edu.cn

ABSTRACT: Understanding the role of underlying sand layers in stratified soils is essential for clarifying liquefaction mechanisms under high-stress conditions. Previous studies have primarily focused on the effects of low-permeability interlayers; however, the influence of the thickness of the underlying sand layer on pore water pressure redistribution and artesian response remains insufficiently understood. In this study, two centrifuge shaking table tests were conducted under unequal stress similarity conditions to investigate the dynamic responses of layered foundations with different underlying sand layer thicknesses. The results indicate that the thickness of the underlying sand layer governs not only the magnitude but also the persistence of excess pore water pressure. A thicker underlying sand layer acts as a pressure reservoir, promoting the development of upward hydraulic gradients and sustaining artesian pressure, which leads to delayed pore pressure dissipation, deeper liquefaction development, and significant weakening of the overlying soils. These findings demonstrate that the underlying sand layer plays a critical role in liquefaction under constrained drainage conditions and highlight its importance in seismic design and liquefaction risk assessment of deep stratified foundations.

1 INTRODUCTION

Deep overburden foundations are widely distributed in seismically active regions worldwide, including California in the United States, the Kanto Plain in Japan, and the Canterbury Basin in New Zealand, and commonly contain low-permeability fine-grained interlayers such as silt or silty clay (Youd et al., 2001; Seed et al., 2003; Cubrinovski et al., 2011; van Ballegooy et al., 2014). These deposits typically reach thicknesses of several tens to several hundreds of meters and serve as critical foundation conditions for major infrastructures such as high dams, tunnels, and underground structures Under strong seismic loading (Lin et al., 2015; Cui et al., 2022), deep overburden foundations are prone to pore water pressure accumulation, liquefaction, and post-earthquake differential deformation, posing significant challenges to seismic safety.

In stratified sandy deposits, fine-grained interlayers with low permeability significantly alter the hydraulic response of the soil system during seismic loading. These interlayers act as drainage barriers, restricting the dissipation of pore water pressure and promoting its accumulation in adjacent sand layers (Fiegel and Kutter, 1994; Kokusho, 2000; Kokusho, 2003). As a result, excess pore water pressure tends to localize near the interlayer, leading to delayed dissipation, the formation of water films, and strength degradation in both the overlying and underlying soils (Lee et al.,2014). Under such conditions, liquefaction development is governed not only by cyclic loading but also by drainage restriction induced by the interlayer.

Although these mechanisms have been extensively investigated through laboratory tests and centrifuge modeling, most previous studies have focused on relatively shallow deposits, limiting their applicability to deep overburden conditions. In such stratified systems, the sand layer beneath the interlayer plays a critical role in the generation and redistribution of pore water pressure. Its thickness directly affects both the storage capacity and transmission pathways of pore water pressure, thereby controlling the development of upward hydraulic gradients and artesian response beneath the interlayer (Wen et al., 2025). A thicker underlying sand layer provides a larger storage volume for pore water pressure and facilitates the formation of sustained upward hydraulic gradients, which promotes the accumulation and persistence of excess pore water pressure, enhances artesian effects, and intensifies soil weakening.

However, despite its critical role, the influence of underlying sand layer thickness on artesian pressure development, pore pressure evolution, and liquefaction patterns remains insufficiently understood. To address this issue, this study conducts high-g centrifuge shaking table tests under unequal stress similarity conditions to comparatively investigate the seismic response of layered foundations with different underlying sand layer thicknesses. Particular attention is given to artesian response, pore pressure redistribution, and the associated liquefaction mechanisms, with the aim of clarifying the governing processes of limited drainage condition in deep stratified sandy deposits.

2 PROCEDURE OF PHYSICAL MODEL TESTS

To investigate the influence of underlying sand layer thickness on pore water pressure evolution and liquefaction behavior of layered foundations under high initial stress conditions, two high-g centrifuge shaking table tests were conducted, referred to as Model A and Model B. The configurations of the two models are shown in Fig.1.

Following the " modelling of models" concept (Tobita et al.,2011), the model geometry and layer thicknesses were carefully configured such that equivalent prototype stress conditions were achieved at corresponding depths in both models, enabling a consistent comparison under different underlying sand thicknesses. Both models incorporate a low-permeability fine-grained interlayer, while the thickness of the underlying sand layer beneath the interlayer was varied as the only control parameter.Model A represents a layered deep overburden foundation with a relatively thin underlying sand layer, whereas Model B adopts an identical configuration except for a thicker underlying sand layer. By comparatively analyzing the dynamic responses of the two models under seismic loading, this study aims to clarify the role of underlying sand thickness in controlling drainage conditions, artesian pressure development, and liquefaction patterns.

2.1 Test material

As shown in Fig.3, the sand and silt used in the centrifuge model tests were selected to be representative of the prototype soils. Their grain size distribution curves are presented in Fig.2, and other physical properties are summarized in Table 1. To address the inconsistency in time scaling between seismic loading and the consolidation process, a high-viscosity fluid was used to saturate the models (Dewoolkar et al., 1999). Silicone oil was selected as the pore fluid, and the target kinematic viscosity for both Model A and Model B was 120 cSt.

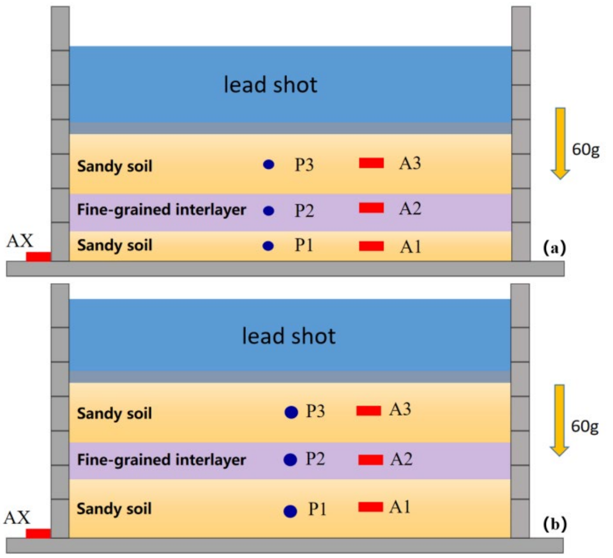

Figure 1.Two centrifuge shaking table tests :(a) Layered foundation with a thin underlying sand layer(b)Layered foundation with a thick underlying sand layer

2.2 Model preparation

As illustrated in Fig. 4, to minimize boundary effects, the model was prepared in a laminar container with internal dimensions of 740 mm in length, 340 mm in width, and 425 mm in depth. The sand layers were constructed using the air pluviation method, with a target dry density of ρ_d=1619 kg/m³, corresponding to a relative density of D_r=60% at the prototype scale. The sandy silt layer was prepared as a pre-fabricated and fully saturated fine-grained soil layer, corresponding to a prototype void ratio of e = 0.86.The achieved density was calculated by the measurements of soil mass and volume.To ensure full saturation of the model, vacuum saturation was carried out in stages after the preparation of each sand layer, allowing pore fluid to adequately infiltrate the soil mass.

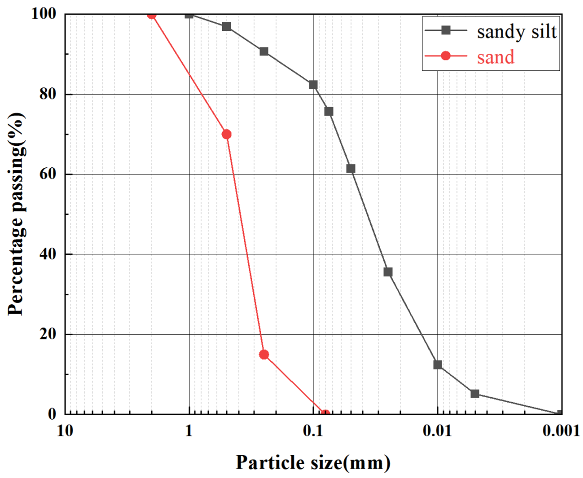

Figure 2.Grain size distribution curve of tested soil

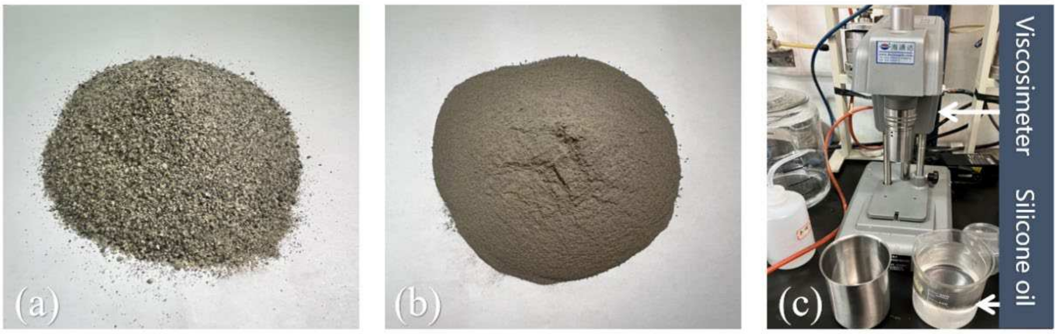

Figure 3.Test materials: (a) test sand; (b) test sandy silt; (c) silicone oil preparation.

Table. 1 Physical properties and grain size distribution parameters of tested soil.

Soil type	G_s(g/cm^3)	D_r/e	D_{50}(mm)	C_u	C_c	K (m/s)
sand	2.644	60%	0.377	3.61	1.37	4e-5
sandy silt	2.72	0.86	0.035	10.81	1.11	7e-8

2.3 The state parameter-based centrifuge scaling law

Both tests in this study were conducted in accordance with the state parameter-based centrifuge scaling law, the detailed derivation of which can be found in Ma (2022). Using the identical initial state along the entire depth, the model and the prototype can demonstrate consistent normalized stress-strain behavior. Given the geometry scaling factor λ, the scaling factor of acceleration N^{-1}, the scaling factor of soil density λ_ρ, and assuming that the variation in void ratio has a negligible effect on the density and permeability of the soil in the model, the state parameter-based centrifuge scaling law could be derived in Table 2.

3 SENSOR RESPONSES IN THE MODEL

The Arias intensity (I_a) was adopted to quantitatively evaluate the energy intensity of the input ground motions (Campbell and Bozorgnia, 2012). The definition of the Arias intensity is given as follows.

$$I_a = \frac{\pi}{2g}\int_0^{t_0} a^2\,(t)\,dt \tag{1}$$

where a(t) represents the time history of the acceleration, and t_0 is the duration of the acceleration.

Figure 5 presents the acceleration and Arias intensity time histories recorded at the shaking table base under 0.45 g sinusoidal excitation (15 cycles). The evolution of Arias intensity is nearly identical for both models, indicating good consistency in the input seismic energy. Minor differences in the accumulation rate are negligible, confirming the reliability of subsequent comparative analyses.

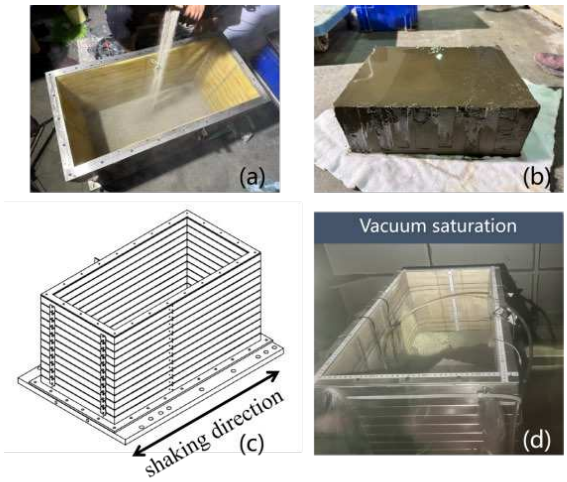

Figure 4.Model preparation: (a) sand layer preparation procedure; (b) pre-fabricated sandy silt layer; (c) laminar container; (d) vacuum saturation procedure

Table. 2 The scaling factors used in the experiments

Physical quantities	Dimension	Scaling factors	Model A、B (λ=240, N=60)
Geometry	L	λ	240
Density	ML^{-3}	λ_ρ	1
Time	T	$\lambda^{0.5} N^{0.5}$	120
frequency	T^{-1}	$\lambda^{-0.5} N^{-0.5}$	1/120
Acceleration	LT^{-2}	N^{-1}	1/60
Velocity	LT^{-1}	$\lambda^{0.5} N^{-0.5}$	2
Displacement	L	λ	240
Stress	$ML^{-1}T^{-2}$	$\lambda\lambda_\rho N^{-1}$	4
Strain	-	1	1
Viscosity	L^2T^{-1}	$\lambda^{-0.5} N^{-0.5}$	2
pore water pressure	$ML^{-1}T^{-2}$	λN^{-1}	4

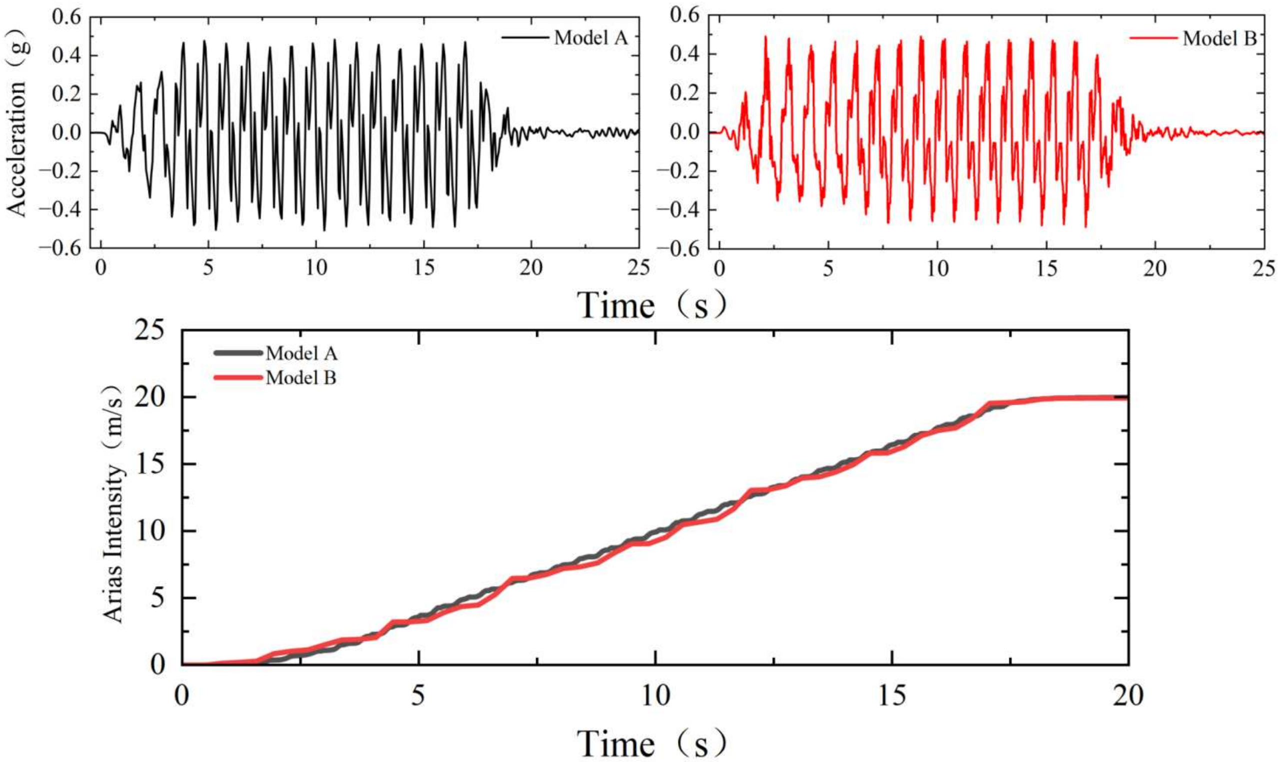

Figure 5.Arias intensity time histories at the base

Figure 6 presents the time histories of excess pore water pressure recorded at different locations in Models A and B during seismic loading. The monitoring points P1, P2, and P3 are located within the underlying sand layer, near the interlayer, and above the interlayer, respectively. By comparing the buildup, oscillation, and post-shaking dissipation of excess pore water pressure at different depths, the influence of underlying sand layer thickness on pore pressure evolution and liquefaction behavior in layered foundations can be systematically evaluated.

At the P3 location above the interlayer, both models exhibit rapid excess pore water pressure accumulation and pronounced cyclic oscillations during seismic shaking (0–30 s), indicating that the overlying sand layer quickly reaches a high pore pressure state under cyclic shearing. During this stage, pore pressure response is primarily governed by seismic input, and the influence of underlying sand thickness on peak values is relatively limited. After shaking ceases, however, Model B with a thicker underlying sand layer shows noticeably delayed pore pressure dissipation compared with Model A, suggesting a sustained influence of artesian pressure and drainage-path control from the underlying sand layer.

At the P2 location near the interlayer, the contrast between the two models is most pronounced. During seismic shaking, Model B consistently exhibits higher excess pore pressure levels and larger oscillation amplitudes than Model A, indicating continuous pore pressure supply from the thick underlying sand layer. In the post-shaking stage, Model B displays a clear high-pressure plateau, with excess pore water pressure maintained at elevated levels for an extended period, whereas pore pressure in Model A dissipates rapidly. These observations demonstrate that under drainage restriction imposed by the low-permeability interlayer, the thickness of the underlying sand layer plays a dominant role in controlling pore pressure evolution near the interlayer.

At the P1 location within the underlying sand layer, the influence of sand layer thickness is most direct and pronounced. Model B exhibits both higher peak excess pore water pressure and significantly slower post-shaking dissipation, maintaining substantial positive excess pore water pressure for a prolonged duration. In contrast, Model A shows limited peak pore pressure and much faster dissipation. These results indicate that under high initial stress conditions, a thickened underlying sand layer acts as a primary artesian pressure reservoir, intensifying deep pore pressure accumulation and persistence rather than mitigating liquefaction response.

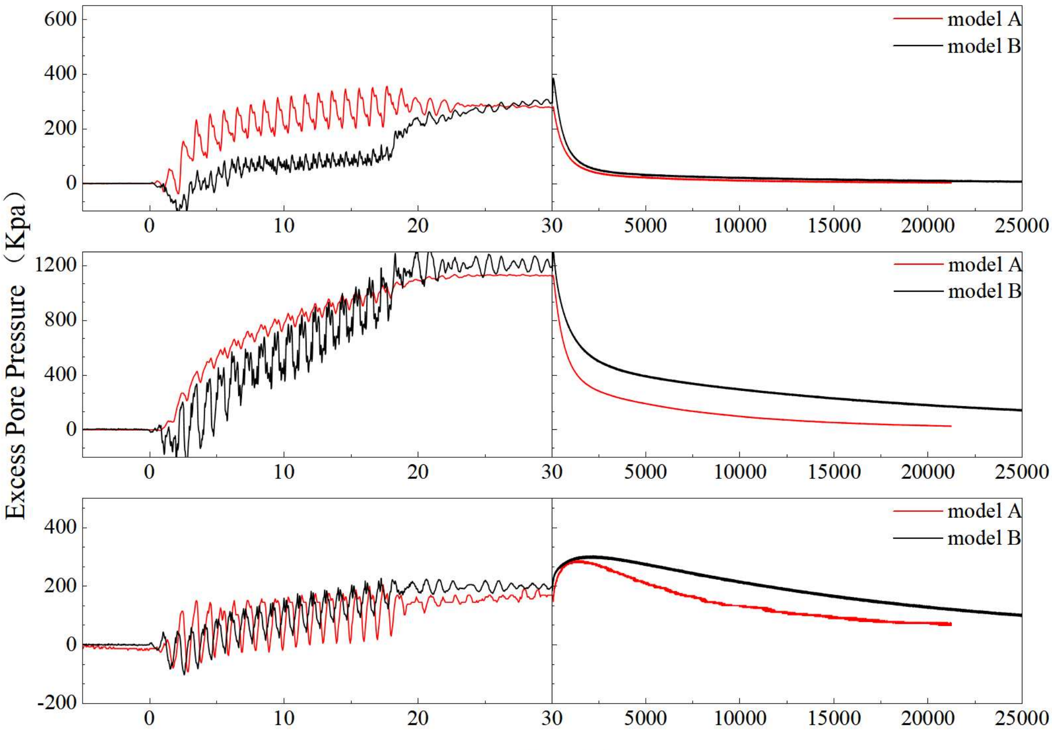

Figure 6.Model preparation: (a) sand layer preparation procedure; (b) pre-fabricated sandy silt layer; (c) laminar container; (d) vacuum saturation procedure

4 CONCLUSIONS

This study conducted two high-g centrifuge shaking table tests under unequal stress similarity conditions to investigate the influence of underlying sand layer thickness on pore water pressure evolution and liquefaction behavior in layered foundations subjected to high initial stress conditions. Based on the experimental observations, the following conclusions can be drawn:

(1) Under high initial stress conditions, layered foundations containing a low-permeability interlayer exhibit characteristics of limited drainage condition, with rapid excess pore water pressure buildup during seismic shaking and pronounced post-shaking dissipation delay.

(2) The thickness of the underlying sand layer plays a critical role in governing the spatial and temporal evolution of pore water pressure. A thicker underlying sand layer promotes the development of sustained artesian pressure, delays pore pressure dissipation, enhances excess pore pressure persistence at depth and near the interlayer, and facilitates upward transmission of liquefaction effects. In contrast, a thinner underlying sand layer allows faster pore pressure

release, limits artesian effects, and results in more localized liquefaction development.

(3) Under high initial stress conditions, thickening the underlying sand layer does not mitigate liquefaction response; instead, due to its larger volume and greater water storage capacity, it acts as a primary artesian pressure reservoir, intensifying deep pore pressure accumulation and prolonged post-earthquake weakening.

These findings demonstrate that underlying sand layer thickness is a key controlling factor in the liquefaction behavior and post-earthquake stability of deep layered foundations, providing valuable physical insights for liquefaction risk assessment and seismic design of dam foundations in complex stratified ground conditions.

ACKNOWLEDGEMENTS

This study is supported by the National Natural Science Foundation of China (Nos. 52588202,52278374)and the National Key Research and Development Program of China (Nos. 2024YFF1700901, 2024YFF1702003). The authors would thank Dr. Yuan Cao Mr. Zizhuang Yan, Mr. Shuai Hong of Zhejiang University for their great help during the centrifuge model tests.

REFERENCES

Youd, T.L., and I.M. Idriss (2001). Liquefaction resistance of soils: Summary report from the 1996 NCEER and 1998 NCEER/NSF workshops on evaluation of liquefaction resistance of soils. *Journal of Geotechnical and Geoenvironmental Engineering*, 127(4), 297–313. http://doi.org/10.1061/(ASCE)1090-0241(2001)127:4(297)

Seed, R.B., K.O. Cetin, R.E.S. Moss, A.M. Kammerer, J. Wu, J.M. Pestana, M.F. Riemer, R.B. Sancio, J.D. Bray, R.E. Kayen, and A. Faris (2003). *Recent advances in soil liquefaction engineering: A unified and consistent framework*. Earthquake Engineering Research Center Report No. EERC 2003-06, University of California, Berkeley.

Cubrinovski, M., J.D. Bray, M. Taylor, S. Giorgini, B. Bradley, L. Wotherspoon, and J. Zupan (2011). Soil liquefaction effects in the central business district during the February 2011 Christchurch earthquake. *Seismological Research Letters*, 82(6), 893–904. http://doi.org/10.1785/gssrl.82.6.893

van Ballegooy, S., P. Malan, V. Lacrosse, M.E. Jacka, M. Cubrinovski, J.D. Bray, T.D. O' Rourke, S.A. Crawford, and H. Cowan (2014). Assessment of liquefaction-induced land damage for residential Christchurch. *Earthquake Spectra*, 30(1), 31–55. http://doi.org/10.1193/021413EQS050M

Lin, P., B. Huang, Q. Li, and R. Wang (2015). Hazard and seismic reinforcement analysis for typical large dams following the Wenchuan earthquake. *Engineering Geology*, 194, 86–97. http://doi.org/10.1016/j.enggeo.2015.05.010

Cui, P., Y. Ge, S. Li, Z. Li, X. Xu, G.G.D. Zhou, H. Chen, H. Wang, Y. Lei, L. Zhou, S. Yi, C. Wu, J. Guo, Q. Wang, H. Lan, M. Ding, J. Ren, L. Zeng, Y. Jiang, and Y. Wang (2022). Scientific challenges in disaster risk reduction for the Sichuan–Tibet Railway. *Engineering Geology*, 309, 106837. http://doi.org/10.1016/j.enggeo.2022.106837

Fiegel, G.L., and B.L. Kutter (1994). Liquefaction mechanism for layered soils. *Journal of Geotechnical Engineering*, 120(4), 737–755. http://doi.org/10.1061/(ASCE)0733-9410(1994)120:4(737)

Kokusho, T. (2000). Mechanism for water film generation and lateral flow in liquefied sand layer. *Soils and Foundations*, 40(5), 99–111. http://doi.org/10.3208/sandf.40.5_99

Kokusho, T. (2003). Current state of research on flow failure considering void redistribution in liquefied deposits. *Soil Dynamics and Earthquake Engineering*, 23(7), 585–603. http://doi.org/10.1016/S0267-7261(03)00077-9

Lee, C.J., H.T. Chen, H.C. Lien, Y.C. Wei, and W.Y. Hung (2014). Centrifuge modeling of the seismic responses of sand deposits with an intra-silt layer. *Soil Dynamics and Earthquake Engineering*, 65, 72–88. http://doi.org/10.1016/j.soildyn.2014.05.012

Wen, S., X. Wei, G. Sheng, and X. Ni (2025). Dynamic behavior and deformation mechanisms of sand–silt stratified soil under intermittent cyclic loading. *Soil Dynamics and Earthquake Engineering*, 196, 109509. http://doi.org/10.1016/j.soildyn.2025.109509

Tobita, T., S. Iai, L. von der Tann, and Y. Yaoi (2011). Application of the generalised scaling law to saturated ground. *International Journal of Physical Modelling in Geotechnics*, 11(4), 138–155. http://doi.org/10.1680/ijpmg.2011.11.4.138

Dewoolkar, M.M., H.Y. Ko, A.T. Stadler, and S.M.F. Astaneh (1999). A substitute pore fluid for seismic centrifuge modelling. *Geotechnical Testing Journal*, 22(3), 196–210. http://doi.org/10.1520/GTJ11111J

Ma, Q., Y.G. Zhou, X.T. Yang, and Y.M. Chen (2022). A state parameter-based scaling law for centrifuge modelling. *Soil Dynamics and Earthquake Engineering*, 162, 107487. http://doi.org/10.1016/j.soildyn.2022.107487

Campbell, K.W., and Y. Bozorgnia (2012). A comparison of ground motion prediction equations for Arias intensity and cumulative absolute velocity developed using a consistent database and functional form database. *Earthquake Spectra*, 28(3), 931–941. http://doi.org/10.1193/1.4000067